AGU100 ADVANCING EARTH AND SPACE SCIENCE

Geophysical Research Letters

RESEARCH LETTER

10.1029/2018GL078758

Gas Transfer by Breaking Waves

Luc Deike[1,2] and W. Kendall Melville[3]

[1]Department of Mechanical and Aerospace Engineering, Princeton University, Princeton, NJ, USA, [2]Princeton Environmental Institute, Princeton University, Princeton, NJ, USA, [3]Scripps Institution of Oceanography, University of California San Diego, La Jolla, CA, USA

Key Points:

- We present a bubble-mediated gas transfer theory that accounts for the breaking wave dynamics and statistics
- We develop a general spectral formulation for gas transfer that can be implemented in large-scale wave-ocean coupled models
- We present a semiempirical formulation for CO_2 and DMS gas transfer that collapses all available data and that can be applied to other gases

Correspondence to:
L. Deike,
ldeike@princeton.edu

Citation:
Deike, L., & Melville, W. K. (2018). Gas transfer by breaking waves, *Geophysical Research Letters*, *45*, 10,482–10,492. https://doi.org/10.1029/2018GL078758

Received 15 MAY 2018
Accepted 10 SEP 2018
Accepted article online 17 SEP 2018
Published online 2 OCT 2018

Abstract

The transfer of gases at the ocean-atmosphere interface impacts weather and climate from local to global scales, with carbon dioxide (CO_2) key to marine life and ecosystems, and dimethyl sulfide affecting aerosols and atmospheric processes. However, the bubble-mediated gas transfer, associated with breaking waves has remained poorly constrained. We present a spectral framework for bubble-mediated gas transfer, computed from a mechanistic model for air bubble entrainment at the breaking wave scale combined with a chemical model. Gas transfer is upscaled to the ocean scale by evaluating air entrainment at all wave scales using wave and wave breaking statistics. The obtained CO_2 gas transfer velocity reproduces the variability of historical parameterizations and recent field measurements, with very good accuracy. We propose a wind-wave parameterization that collapses all available data, which can be directly implemented in ocean-wave models or used with remote sensing of the ocean surface to infer gas transfer.

Plain Language Summary

The transfer of gases at the ocean-atmosphere interface impacts weather and climate from local to global scales. The exchanges of carbon dioxide and oxygen are key to marine life and ecosystems, while transfer of dimethyl sulfide has a strong effect on aerosol composition, affecting atmospheric processes. Yet the bubble-mediated gas transfer, associated with breaking waves has remained poorly constrained. We present a general framework for gas transfer in the open ocean, where air entrainment and the associated bubble-mediated gas transfer are evaluated at all scales. We combine a mechanistic model for air entrainment and bubble statistics at the breaking wave scale with a chemical model for gas transfer by the entrained air bubbles and then upscale the gas exchange using the wave and wave breaking statistics. The obtained gas transfer velocity for CO_2 reproduces the variability of historical parameterizations and recent field measurements, with very good accuracy, and we propose a wind-wave parameterization that collapse all available data. The proposed model for gas transfer can be directly implemented in coupled ocean-wave models, or used with remote sensing data of the ocean surface to infer gas transfer, strongly improving predictions of gas exchange at the ocean-atmosphere interface.

1. The Role of Wave Breaking in Ocean-Atmosphere Gas Exchange

Physical processes at the ocean-atmosphere interface have a large effect on climate and weather by controlling the transfer of momentum and mass. Without wave breaking, transport between the ocean and the atmosphere is through slow conduction and molecular diffusion, while wave breaking is a transitional process from laminar to turbulent flow. When waves are breaking, the surface experiences dramatic changes, with sea spray ejection in the atmosphere and air entrainment into the ocean water. The complex dynamics and statistics of wave breaking in a particular ocean location depends mainly on the local wave state not the wind velocity, while current parameterizations for ocean-atmosphere interactions are based almost exclusively on the wind speed.

Ocean uptake accounts for approximatively 30% of the CO_2 released into the atmosphere, and carbonic acid forms CO_2 in solution, causing ocean acidification, impacting shell-forming marine animals (Rhein et al., 2013). The contribution of bubble-mediated transfer remains to be clarified. The gas transfer at the ocean-atmosphere interface is calculated from the gas concentrations in the air and water, expressed as a function of the gas solubility, α, and partial pressure in the water, p_w, and in the air, p_a (Wanninkhof et al., 2009),

$$F = k_w \alpha (p_w - p_a), \tag{1}$$

where k_w is the gas transfer velocity, which depends on the physicochemical properties (solubility and diffusivity D) of the gas and the atmospheric and oceanic conditions. State-of-the-art ocean-atmosphere parameterizations for the transfer velocity, used in ocean and climate models (Fairall et al., 2003, 2011), include a Schmidt number scaling (typically, $k_w \propto Sc^{-1/2}$, $Sc = \nu/D$, where ν is the kinematic viscosity) but depend solely on wind speed to account for turbulent and wave breaking-induced transfers. Recent open ocean gas transfer velocity measurements of CO_2 and dimethyl sulfide (DMS) display very large scatter, when analyzed as a function of wind speed (Bell et al., 2017; Brumer et al., 2017; Edson et al., 2011; Garbe et al., 2014; Miller et al., 2009), exposing the failure of wind speed parameterization at intermediate to high wind speeds, which is associated with bubble-mediated gas transfer. Separating the contribution to the total flux into the bubble gas transfer and the diffusive transfer at an unbroken surface, bubble-mediated gas transfer is introduced through the whitecap coverage (Asher et al., 1996; Keeling, 1993; Woolf, 1997, 2005; Woolf & Thorpe, 1991), which is ultimately described by a function of the wind speed. Liang et al.(2011, 2012, 2013) proposed an approach to consider bubble-mediated gas fluxes, through a hierarchy of models, going from numerical simulations at the bubble scale, to large eddy simulations, to climate models. However, the final parameterization remains based on wind speed only when moving to ocean and climate models, losing the variability in gas transfer induced by the wave state. Toba et al. (2006) and Brumer et al. (2017) proposed mixed empirical parametrization using a wave-based Reynolds number considering both wind speed and significant wave height and show a reduction in the scatter of gas transfer velocity data, without providing a rationale for the obtained empirical relationships.

A general theoretical framework going consistently from the bubble scale to the final gas transfer velocity, and its dependence on wind and wave parameters has remained elusive, due to the complex nature of breaking and air entrainment, a two-phase turbulent process, and the very large range of scales involved in the process, from wave statistics scales of order of kilometers, O(1 km), to wave breaking dynamics, O(1 – 10 m), air entrainment, bubble generation, and dissolution O(centimeters to micrometers). We proposed a model for air entrainment and bubble statistics as a function of the wave variables, combining high-fidelity direct numerical simulations and laboratory measurement (Deike et al., 2016). We combined our one wave model with the measured wave and wave breaking statistics and proposed a formulation for the volume flux of air entrained by breaking waves in the ocean (Deike et al., 2017). Here by integrating the gas transfer model from Keeling (1993) to our approach, we present a formulation for the bubble-mediated gas transfer due to breaking waves, taking into account processes at all scales. This theory is for the transfer of any gas, and could be implemented in coupled wave-ocean-atmosphere and climate models, which should significantly reduce the uncertainties at moderate to high wind speeds. Finally, we propose a simple parameterization for the case of CO_2, as a function of wind friction velocity and wave height, solubility, and diffusivity, derived from the full equation, that collapses all available data.

2. A Spectral Model for Gas Transfer by Breaking Waves

We present a spectral formulation for the bubble-mediated gas transfer, based on assumptions made to the best of our current knowledge, combining a bubble gas transfer model (Keeling, 1993) and our model for air entrainment by breaking waves (Deike et al., 2016, 2017).

The distribution of the average breaker front length, $\Lambda(c)$, introduced by Phillips (1985), and defined per unit area of sea surface per unit increment of breaking front velocity c, describes the breaking statistics. We work under the assumption of alignment of the wind and wave directions. The wave statistics are represented by the wave spectrum $\phi(k)$, that is, the wave energy density as a function of the wave number. The dispersion relation of ocean gravity waves in deep water relates the wave phase speed and the wave number, $c = \sqrt{g/k}$, where g is the gravitational acceleration. Note that the breaking front has been observed to move at a velocity v below the phase velocity, $0.8c \leq v \leq c$, which can lead to significant differences in the higher moments, but a general theoretical description of the speed of the breaking front for various wind and wave conditions is still lacking (Banner & Peirson, 2007; Banner et al., 2014; Kleiss & Melville, 2010; Rapp & Melville, 1990; Romero et al., 2012).

Deike et al. (2017) have demonstrated that the volume flux of air entrained by breaking waves (volume per unit time, per unit ocean surface area), V_A, is given by the slope-modulated third moment of $\Lambda(c)$,

$$V_A = \int v_l(c)\Lambda(c)\mathrm{d}c, \text{ with } v_l(c) = \mathcal{B}\chi s(k)^{3/2}\frac{c^3}{g}, \quad (2)$$

where $v_l(c)$ is the volume flux per unit length of breaking crest, $s(k)$ is the scale-dependent wave slope above breaking, which is calculated from the saturation spectrum $B(k) = \phi(k)k^3$, and χ is a nondimensional constant to ensure a closed energy dissipation budget (Drazen et al., 2008; Romero et al., 2012). $\mathcal{B} = 0.1 \pm 0.05$ is the bubble plume constant accounting for the balance between the mechanical dissipation and the work done by buoyancy forces (Deike et al., 2016). Equation (2) can be integrated using wave and wave breaking statistics from field measurements (Deike et al., 2017) or directly evaluated in coupled ocean-wave models.

The bubble-mediated transfer is directly related to the flux of bubbles being entrained, defined as the number per unit ocean surface area per unit time, $Q(r)$, related to the air volume flux by

$$Q(r) = \int q_l(r, c)\Lambda(c)\mathrm{d}c, \text{ with } q_l(r, c) = \frac{\mathcal{B}}{2\pi}\chi s(k)^{3/2} n(r)\frac{c^3}{g}, \tag{3}$$

where $q_l(r, c)$ is the size-dependent bubble flux per unit length of breaking crest. The bubble size distribution (number per unit bubble radius per unit volume) $n(r)$ is separated into two parts. For bubbles larger than the Hinze scale, r_{H}, defined as the scale for which surface tension prevents bubble breakup by turbulence (Deane & Stokes, 2002; Garrett et al., 2000), $r > r_{\mathrm{H}}$, $n(r) = n_1 r_{\mathrm{m}}^{-2/3} r^{-10/3}$, with r_{m} the maximum entrained bubble size, and n_1 a nondimensional constant (Deike et al., 2016). Following Deane and Stokes (2002) and Liang et al. (2011), we assume that 95% of the bubble volume is due to bubbles with $r > r_H$. For $r < r_{\mathrm{H}}$, $n(r) = n_2 r^{-2/3}$, where n_2 is a dimensional factor to assure continuity of the bubble size distribution, and we use the large-scale constraints on the total volume flux, equation (2), and $V_A = \int \mathrm{d}r Q(r)\frac{4\pi}{3}r^3$, to determine n_1 and n_2.

Following Keeling (1993), we link the outgasing gas transfer velocity from the bubbles to the ocean with the entrained flux of bubbles by breaking waves:

$$K_b^{\mathrm{out}} = \iint \mathrm{d}c\mathrm{d}r f_l(r, c)\Lambda(c), \text{ with } f_l(r, c) = \frac{q_l(r, c)E(r)}{\alpha}, \tag{4}$$

where $f_l(c)$ is the bubble-mediated gas transfer per unit length of breaking crest due to breaking waves moving at speeds between c and $c + \mathrm{d}c$, α is the Ostwald gas solubility, and $E(r)$ is a nondimensional efficiency factor related to the initial depth of entrainment of the bubble z_0 and an equilibrium depth $H_{\mathrm{eq}}(r)$, given by Keeling (1993):

$$E(r) = \frac{z_0}{z_0 + H_{\mathrm{eq}}(r)} \text{ and } H_{\mathrm{eq}}(r) = \frac{4\pi}{3\alpha}\frac{r w_b(r)}{k_b(r)}. \tag{5}$$

Dense bubble clouds have been observed to be entrained to depths comparable to the breaking wave heights, which, in the field, we assume can be scaled by the significant wave height, $z_0 \approx H_s$ (Lenain & Melville, 2017a). Following laboratory experiments and numerical simulations, we assume that the bubble size distribution does not initially depend on the depth over the breaking height (Deane & Stokes, 2002; Deike et al., 2016; Lamarre & Melville, 1991). The equilibrium depth $H_{\mathrm{eq}}(r)$ is a function of the bubble rise velocity in the turbulent upper ocean, $w_b(r)$, and the exchange velocity for a single bubble, $k_b(r)$, which are functions of the bubble radius and the gas physicochemical properties. Following Woolf and Thorpe (1991) and Keeling (1993), we consider the exchange velocity for a clean bubble,

$$k_b(r) = 8\sqrt{\frac{\pi D w_b(r)}{2r}}. \tag{6}$$

There is limited information on the rise velocity in turbulent ocean water, with reports of rise velocities in turbulence between 30% and 70% lower than the value in clean water (Aliseda & Lasheras, 2011; Loisy & Naso, 2017). We follow Thorpe (1982) and Keeling (1993) and consider the rise velocity in dirty water, as contaminants are present in ocean water and reduce the rise velocity of the bubbles

$$w_b(r) = \frac{2r^2 g}{9\nu_w}\left[(\upsilon^2 + 2\upsilon)^{1/2} - \upsilon\right], \text{with} \upsilon = 10.82/\chi, \text{and} \chi = \frac{g r^3}{\nu_w^2}. \tag{7}$$

We retain the chemical gas exchange model from Keeling (1993) but make significant improvements to the underlying physics of air entrainment. We use an accurate bubble size distribution supported by experimental and numerical data, and theoretical analysis. We consider for the depth of penetration, $z_0 = H_s$, which can be evaluated from the actual wavefield. Moreover, we consider directly the measured wave and wave breaking statistics and not an empirical relationship between air entrainment, whitecap coverage, and wind speed.

From the physicochemical properties of the gas (solubility, diffusivity, and viscosity) and the wave and wave breaking statistics, we can compute the bubble outgassing velocity by integrating equation (4) which in its final form reads,

$$K_b^{out} = \iint dcdr \frac{\mathcal{B}\chi}{2\pi} \frac{s(k)^{3/2} c^3 \Lambda(c)}{g} \frac{n(r)E(r)}{\alpha}. \tag{8}$$

A simple parameterization can be derived by using semiempirical models for the wave and wave breaking statistics. To compare our results with measured gas transfer velocities, we use a parameterization for the nonbreaking gas transfer component, due to molecular diffusion enhanced by turbulence, K_{nb}, and the total gas transfer velocity is

$$k_w = K_{nb} + K_b^{\text{out}}. \tag{9}$$

3. Predicting the Gas Transfer Velocity From Wave and Wind Measurements

We use our theoretical model to compute the gas transfer velocity of CO_2, directly considering the influence of the sea state.

The nonbreaking flux, K_{nb}, is estimated using the COARE 3.1 parameterization (Fairall et al., 2011) and depends linearly on the wind stress u_*,

$$k_{nb,660}^{\text{COARE}} = k_{nb}^{\text{COARE}} \left(\frac{Sc}{660}\right)^{1/2} = A_{NB} u_*, \tag{10}$$

where $A_{NB} = 1.55 \times 10^{-4}$ is an empirical constant, corresponding to the parameter $A = 1.5$ in COARE (Fairall et al., 2011), close to the one proposed independently by Jähne et al. (1987) and used in Woolf (2005). This choice of parameter describes relatively well DMS gas transfer in the Brumer et al. (2017) experiment, as bubble-mediated gas transfer for DMS is mostly negligible. The value of the constants equivalent to A_{NB} considered in various studies can vary by about 20%, and further constrains on this parameter remain an active area of research (Katul & Liu, 2017). For CO_2, this parameter is almost independent of the solubility variations related to temperature changes, but it can vary by up to a factor of 2 for DMS depending on temperature, so the parameter A_{NB} is modified accordingly (Fairall et al., 2011).

We present modeled gas transfer data obtained in two ways. First, we compute the bubble-mediated gas transfer using observations of the wave and wave breaking statistics from field experiments (Kleiss & Melville, 2010; Lenain & Melville, 2017a; Romero & Melville, 2010; Sutherland & Melville, 2013), which combine measurements of the wave spectrum $\phi(k)$, averaged length of breaking crests $\Lambda(c)$, significant wave height H_s, wind speed U_{10}, peak speed of the wave spectrum c_p, and friction velocity in the air u_* (section 3.1). Second, we consider two recent data sets of eddy covariance gas transfer where u_*, U_{10}, c_p, and H_s are available (Bell et al., 2017; Brumer et al., 2017), and we use semiempirical relationships for the wave statistics ($\phi(k)$ and $\Lambda(c)$, see section 3.2, to calculate the bubble-mediated gas flux and reproduce the gas transfer measurements.

3.1. Air Entrainment From Field Measurements of $\Lambda(c)$ and $\phi(k)$

The wave spectrum in field experiments is measured from lidar (Kleiss & Melville, 2010; Lenain & Melville, 2017b; Romero & Melville, 2010) or from stereo measurements and wave gauge data (Sutherland & Melville, 2013), and then azimuthally integrated to give the omnidirectional spectrum, $\phi(k)$. The scale-dependent wave slope $s(k)$ above the breaking threshold is calculated from the saturation spectrum $B(k) = \phi(k)k^3$, as $s(k) = (\sqrt{B(k)} - \sqrt{B_T})$. We use the threshold B_T and constant χ, which have been shown to close the energy dissipation budget, with $S_{\text{diss}} = \int b(k)\rho g^{-1} c^5 \Lambda(c) \text{d}c$, and $b(k) = \chi(\sqrt{B(k)} - \sqrt{B_T})^{5/2}$ (Drazen et al., 2008; Romero et al., 2012; Sutherland & Melville, 2013, 2015).

The averaged length of breaking crests, $\Lambda(c)$, is obtained from visible and infrared imagery, both airborne (Kleiss & Melville, 2010; Lenain & Melville, 2017a) and platform-based (Sutherland & Melville, 2013) and shown in Figure 1. In the case of the infrared measurement of $\Lambda(c)$, we consider only the visible part of $\Lambda(c)$ through the following procedure. The peak velocity c_2 of the third moment of $\Lambda(c)$, at which air entrainment is a maximum, is measured from the available visible data, and $c_2 = \chi_2\sqrt{gH_s}$, with $\chi_2 = 0.85 \pm 0.1$ fitted to the data, as shown in Figure 1. Note that no trend is observed when c_2 is plotted as a function of u_*. We observe $2 \leq c_2 \leq 6$ m/s, all in the gravity wave range, where $c = \sqrt{g/k}$. We consider the third moment, which is related to air entrainment (Deike et al., 2017), to avoid the uncertainties related to the large roll-off observed in the visible data of $\Lambda(c)$.

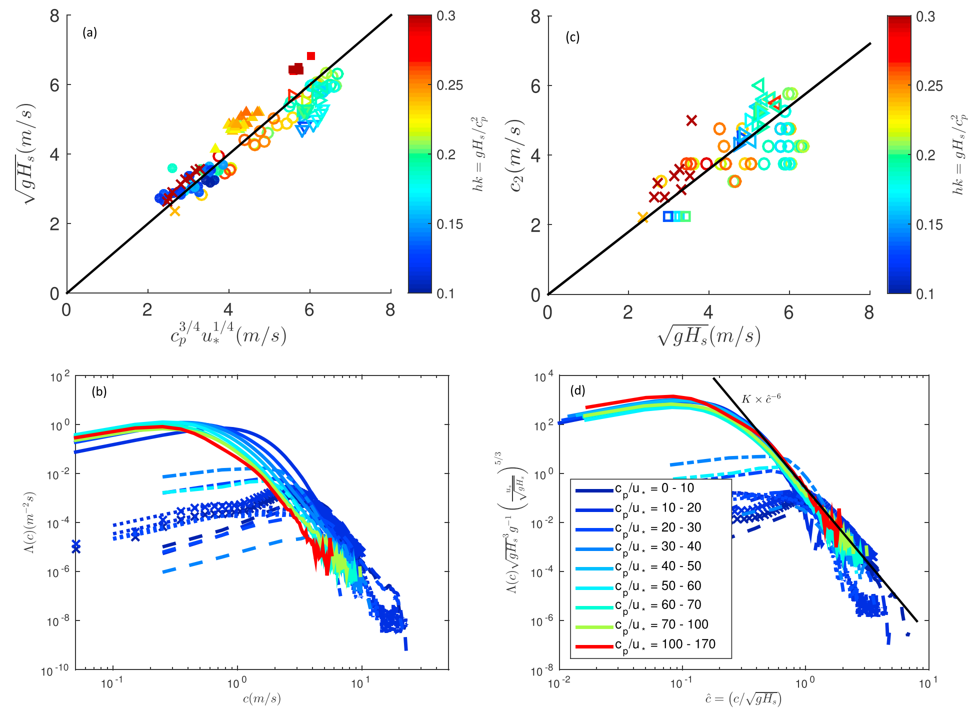

Figure 1. Rationale for modeling the averaged length of breaking crest $\Lambda(c)$. (a) Relationship between the phase speed at the peak of the wave spectrum, c_p, the wind friction velocity and the ballistic velocity, $\sqrt{gH_s}$, proposed by Toba (1972, 1978) for various field experiments, showing the fetch-limited relationship $c_p^{3/4}u_*^{1/4} = \chi_f\sqrt{gH_s}$, with $\chi_f = 1$ fitted to the data (solid line), which is consistent with Toba (1978), where $\frac{gH_s}{u_*^2} = 0.062\left(\frac{gT_p}{u_*}\right)^{3/2}$ and $(2\pi)^{3/2}0.062 = 0.98 \approx \chi_f$. Circles are from Kleiss and Melville (2010), squares from Sutherland and Melville (2013), triangles from Lenain and Melville (2017a), and crosses from Schwendeman et al. (2014) with the global slope color coded. (b) Available data for $\Lambda(c)$, bin-averaged data, by wave age, as presented in Sutherland and Melville (2013). Solid lines are infrared data from RaDyo 2009, SoCal 2010, and HIRES 2010 (Sutherland & Melville, 2013); dashed lines are visible data from GOTEX 2004 and HIRES 2010 (Kleiss & Melville, 2010; Sutherland & Melville, 2013); dotted lines are visible airborne data from HIRES 2010 (Deike et al., 2017; Lenain & Melville, 2017a); and crosses are visible data from Schwendeman et al. (2014). (c) Maxima of $\Lambda(c)$ from the visible imagery measurements, c_2, called the visible low speed limit, as a function of $\sqrt{gH_s}$. Solid line is $c_2 = \chi_2\sqrt{gH_s}$, with $\chi_2 = 0.85$ fitted to the data. Note that no clear correlation is observed between c_2 and u_* (not shown). (d) Proposed scaling for $\Lambda(c)$, adapted from Sutherland and Melville (2013). Solid line is $\frac{\Lambda(c)\sqrt{gH_s}^3}{g} = K\left(\frac{c}{\sqrt{gH_s}}\right)^{-6}\left(\frac{u_*}{\sqrt{gH_s}}\right)^{5/3}$, with $K = 0.25$ fitted to the data.

3.2. Parameterization of $\Lambda(c)$ and $B(k)$

The second type of comparison consists of reproducing recent eddy covariance measurements of the gas transfer velocity performed in the open ocean at moderate to high wind speeds (Bell et al., 2017; Brumer et al., 2017), where measurements of H_s, c_p, and u_* are available. To compute the bubble-mediated gas transfer, we use parameterizations of $\Lambda(c)$ and $\phi(k)$ based on the data set described in section 3.1.

The wind and wave conditions are typically described by u_*, H_s, and c_p. A global wave slope $S = gH_s/c_p^2$ can be defined, with the ballistic velocity of breaking waves, scaled by $\sqrt{gH_s}$, being a parameter of significant importance for the breaking dynamics (Deike et al., 2017; Drazen et al., 2008; Romero et al., 2012). In the field, numerous observations led to fetch-limited relationships, linking the significant wave height and the peak period, (Toba, 1972, 1978; Zakharov et al., 2015), $\frac{gH_s}{u_*^2} = 0.062\left(\frac{gT_p}{u_*}\right)^{3/2}$, with T_p the wave period at the peak of the spectrum, and $c_p = gT_p/(2\pi)$. This relationship is shown in Figure 1 for complex seas and swell conditions (Kleiss & Melville, 2010; Lenain & Melville, 2017a; Schwendeman et al., 2014; Sutherland & Melville, 2013). This suggests that, to leading order, c_p is a function of the two other characteristic velocities of the problem, u_* and $\sqrt{gH_s}$, and therefore, we only need to keep two of them in the dimensional analysis, one being representative of the wind forcing and the other of the wavefield.

The averaged length of breaking crest, $\Lambda(c)$, has been described by Sutherland and Melville (2013) as $\frac{\Lambda(c)c_p^3}{g} = \hat{\chi}\left(\frac{c}{\sqrt{gH_s}}S^{1/10}\right)^{-6}\left(\frac{u_*}{c_p}\right)^{1/2}$, with $\hat{\chi}$ a nondimensional constant fitted to the data. Note that the slope dependency $S^{1/10}$ is very weak and is not necessary to rescale the data. A key success in this result is to rescale c by $\sqrt{gH_s}$, while the c^{-6} relationship is observed over a wide range of scales. Using the fetch-limited relationship, while dropping the $S^{1/10}$ dependency, we can simplify the previous formula to propose a new scaling

$$\frac{\Lambda(c)\sqrt{gH_s}^3}{g} = K\left(\frac{c}{\sqrt{gH_s}}\right)^{-6}\left(\frac{u_*}{\sqrt{gH_s}}\right)^{5/3}, \tag{11}$$

where $K = 0.25 \pm 0.05$ is a nondimensional constant fitted to the data (Figure 1). Note that a similar formula can be obtained, purely by dimensional analysis, seeking the solution $\Lambda(c) = H(c, \sqrt{gH_s}, u_*, g)$, which leads to, $\frac{\Lambda(c)\sqrt{gH_s}^3}{g} = \hat{K}\left(\frac{c}{\sqrt{gH_s}}\right)^{-6}\left(\frac{u_*}{\sqrt{gH_s}}\right)^{\gamma}$, where $\hat{K}$ is a nondimensional constant, and γ is fitted to the data. Due to the difficulty of the measurements and the scatter in the data, acceptable values are between $1.5 \leq \gamma \leq 2$, depending on whether we focus on rescaling the peak in the infrared range, or the peak in the visible range of $\Lambda(c)$, consistent with previous results (Sutherland & Melville, 2013). More field data, as well as theoretical analysis on the breaking statistics, are necessary to further refine the scaling.

We consider a simple parameterization of the omnidirectional wave spectrum $\phi(k)$, based on theoretical arguments (Phillips, 1985; Romero et al., 2012) and field measurements (Lenain & Melville, 2017b; Romero & Melville, 2010). For gas transfer, the most important part of the spectrum is the saturation range, where breaking dominates the dynamics. We consider a spectrum with two characteristic length scales, the peak of the spectrum, k_p, and the transition from equilibrium to saturation k_n. The equilibrium range, for $k_p < k < k_n$, is taken as $\phi(k) = (\beta/2)u_* g^{-1/2}k^{-5/2}$, with β the Toba constant determined empirically, $\beta = 0.016(c_p/u_*)^{0.53}$ (Romero & Melville, 2010). The transition to saturation is given by $k_n = (2\hat{B}/\beta)^2 g u_*^{-2}$, with $\hat{B} = 0.008$ the averaged saturation, and for $k > k_n$, $\phi(k) = \hat{B}k^{-3}$ (Lenain & Melville, 2017b; Romero & Melville, 2010). An empirical roll-off at low wave number ($k < k_p$), $\exp\left[-0.7(k_p/k)^2\right]$, is considered to obtain the correct significant wave height but is irrelevant for the volume flux and gas flux calculation. The final results are sensitive to the saturation value, $\hat{B}$, and the transition wave number k_n, both being relatively poorly constrained in the literature (Lenain & Melville, 2017b; Romero & Melville, 2010).

3.3. Comparison Between the Modeled Gas Transfer and Field Measurements

Figure 2 shows examples of the variables computed in our model, typical of the range covered in our calculations, using field measurements of the wave statistics (Sutherland & Melville, 2013), and the synthetic data reproducing the HiWings and Knorr 2011 conditions from Bell et al. (2017) and Brumer et al. (2017). Figure 2a shows the wave spectrum, $\phi(k)$, and the associated saturation spectrum $B(k) = \phi(k)k^3$. The spectrum exhibits an equilibrium range, where $\phi(k) \propto k^{-5/2}$ and a transition at high wave numbers to the saturation range, where $\phi(k) \propto k^{-3}$. Large variations of the peak spectrum location, the transition to saturation and the saturation value are visible, the last two having a strong impact on the final gas flux. Figure 2b shows the scale-dependent air entrainment $v_l(c)$, with large variations in its amplitude and the velocity at which $v_l(c)$ is a maximum, resulting from the complex interplay between the wave statistics and the averaged length of breaking crest $\Lambda(c)$. The gas flux appears very sensitive to the wave and wave breaking statistics and dynamics, in particular, to the speed and value of the maximum of the breaking distribution $\Lambda(c)$, and the transition and magnitude of the spectral saturation at high wave numbers. Figure 2c shows the bubble rise and exchange velocity for various temperature conditions, while Figure 2d shows the associated equilibrium depth $H_{\mathrm{eq}}(r)$ and efficiency coefficient $E(r)$, in the case of CO_2. The efficiency factor depends on the physicochemical variables but also on the initial depth of the bubble cloud.

We compute the gas transfer velocity for CO_2, normalized by the Schmidt number of 660 (CO_2 at 20 °C) to compare variations in diffusivity, $k_{w660} = (Sc/660)^{1/2}(K_{nb} + K_b^{\mathrm{out}})$. Figure 3a shows that our modeled data, using field measurements of the wave conditions, reproduce the spread in the observed gas transfer data and the range of parameterizations found in the literature (Edson et al., 2011; Ho et al., 2006, 2011; Liss & Merlivat, 1986; Nightingale et al., 2001; Wanninkhof, 1992; Wanninkhof & McGillis, 1999). This suggests that much of the variability in the gas transfer velocity at high wind speeds for CO_2 is related to the particular wave conditions. Moreover, Figure 3b shows that we are able to reproduce the gas transfer measurements from HiWings and Knorr 2011 (Bell et al., 2017; Brumer et al., 2017), within the error bars of the measurements, by using the same approximations for the wavefield in the two data sets. Figure 3c shows all modeled data and recent

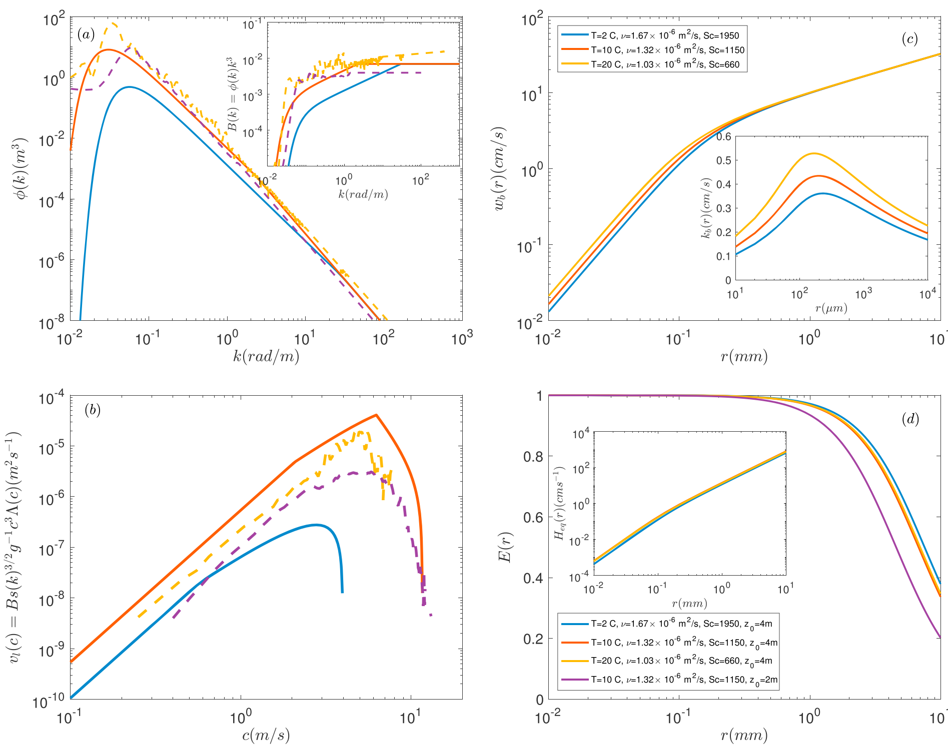

Figure 2. Variables used to compute the bubble-mediated gas transfer. Wave and breaking statistics are shown on the left panels computed from measurements of $\phi(k)$ and $\Lambda(c)$ from field campaigns (dashed lines) and synthetic data reproducing the conditions of HiWings (Brumer et al., 2017) and Knorr 2011 (Bell et al., 2017); solid lines red and blue, respectively). (a) Omnidirectional wave spectrum $\phi(k)$ and associated saturation spectrum $B(k) = \phi(k)k^3$, as a function of wave number. Large variations of the spectrum and its saturation are observed. (b) The scale-dependent volume flux of air entrained by breaking $v_l(c)$ (equation (2)) computed from $\Lambda(c)$ and $B(k)$. Right panels show the modeled chemical exchange variables for CO_2, for various temperature conditions. (c) Modeled rise velocity of bubbles in water, $w_b(r)$ (equation (7)) and modeled transfer velocity $k_b(r)$ (equation (6)) as a function of bubble radius, for increasing temperature, and corresponding decreasing viscosity. (d) Efficiency factor $E(r)$ and equilibration depth $H_{eq}(r)$ as a function of r (equation (5)). The efficiency factor depends on physicochemical variables as well as on the depth of bubble entrainment, $z_0 \approx H_s$.

observations (Bell et al., 2017; Brumer et al., 2017; Edson et al., 2011; Miller et al., 2009). Thus, the modeling approach proposed here is able to reproduce the very large scatter observed in the literature for the CO_2 gas transfer velocity when plotted just against the wind speed and, more specifically, to reproduce particular data sets. In other words, the large scatter in the traditional wind speed dependence of gas transfer is due in large part to the neglect of other physics and physicochemistry that we attempt to address in this paper. Figure 3d shows that the relative bubble-mediated contribution K_b^{out}/k_w for the HiWings and Knorr 2011 modeled data increases with wind speed, as expected. The bubble contribution for CO_2 accounts for more than 40% for $U_{10} \geq 10$ m/s becomes dominant for $U_{10} \geq 15$ m/s and reaches 60% at 20 m/s. Note that these particular numbers depend on the nonbreaking gas transfer parameterization (equation (10)), but the trend would be similar for any choice of $k_{nb} \propto u_*$.

4. Semiempirical Relationship

In an effort to collapse available data sets, Brumer et al. (2017) proposed a mixed parameterization using $R_H = u_* H_s/\nu$ and an empirical relationship for CO_2, $k_{w660} = 2.04 \times 10^{-4} R_H^{0.88}$. However, such fits need to be redone for each particular chemical species, since there is no theoretical framework constraining the exponent and prefactor and viscosity is only used for dimensional purposes. We have seen in Figure 2 that various elements of the wave and wave breaking physics can lead to variations in the final gas flux, which makes a universal empirical relationship difficult to obtain. From our framework, a simplified relationship can be derived, by taking the efficiency factor equal to 1 (largely true for bubbles smaller than 1 mm, see Figure 2), which only affect the physicochemical scalings. The wind and wave scalings are obtained by considering simple models

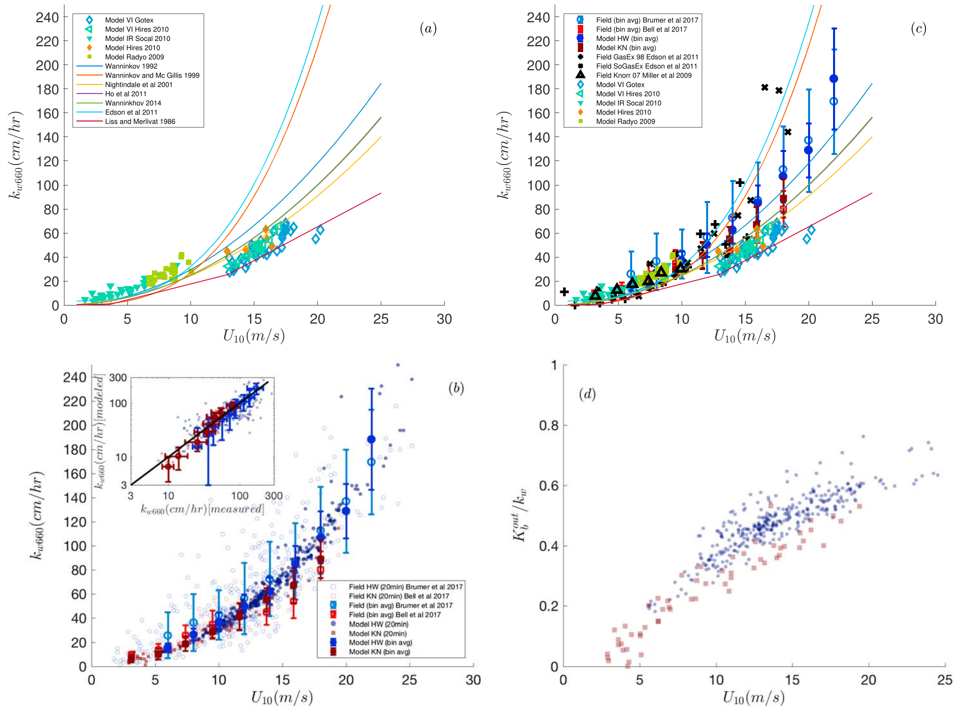

Figure 3. Gas transfer velocity for CO_2, k_{w660}, as of U_{10}. (a) k_{w660} from equations (8) and (9), using field measurements of the wave spectrum $\phi(k)$ and breaking distribution $\Lambda(c)$ from Kleiss and Melville (2010), Sutherland and Melville (2013) and Lenain & Melville, 2017a (IR and VI stand for infrared and visible camera measurements of $\Lambda(c)$, respectively). Solid lines are various empirical relationships based only on wind speed found in the literature (Edson et al., 2011; Ho et al., 2006, 2011; Liss & Merlivat, 1986; Nightingale et al., 2001; Wanninkhof, 1992; Wanninkhof & McGillis, 1999). (b) Modeled and measured k_{w660} from the HiWings (HW; Brumer et al., 2017) and Knorr 2011 (KN; Bell et al., 2017) campaigns. Full symbols are modeled values (blue circles correspond to HW, red squares to KN), while open symbols are the measured values (blue circles; KN: red squares HW). Small symbols are the 20-min averaged data. Large symbols are bin averaged with wind speed U_{10}. The model reproduces the field measurements with good accuracy. Inset shows a comparison between the modeled and measured values (HW: blue circles, KN: red squares). Error bars correspond to the standard deviation of the bin-averaged data. Coefficient of determination for the bin-averaged data are 0.94 (KN) and 0.97 (HW). (c) Available data from various eddy covariance field measurements (Bell et al., 2017; Brumer et al., 2017; Edson et al., 2011; Garbe et al., 2014; Miller et al., 2009), together with the results from our model shown in a and b, with both 20-min averaged and the bin-averaged data for Brumer et al. (2017) and Bell et al. (2017). The modeled data reproduce the spread in k_{w660}. (d) Bubble-mediated contribution to total gas transfer velocity, K_b^{out}/k_w, from modeled data reproducing Brumer et al. (2017) and Bell et al. (2017), as a function of U_{10}. For $U_{10} \geq 10$ m/s, the bubble term can be up to 40% of the total CO_2 gas transfer and becomes dominant for $U_{10} \geq 15$ m/s.

for the wave and wave breaking dynamics. We assume a constant saturation of the spectrum at high wave numbers (Lenain & Melville, 2017b; Romero et al., 2012) and then use the following scaling for the average length of breaking crest, $\Lambda(c) \propto g^{-1}u_*^{\gamma}\sqrt{gH_s}^{\zeta}c^{-6}$, where $\gamma = 5/3$ and $\zeta = 4/3$ and $\zeta + \gamma = 3$ constrained by dimensional analysis (note that when scaling $\Lambda(c)$ empirically, the following ranges of exponents $1.5 \leq \gamma \leq 2$, $1 \leq \zeta \leq 1.5$ are acceptable). This leads to $K_b^{\mathrm{out}} = \tilde{A_B}u_*^{5/3}\sqrt{gH_s}^{4/3}/\alpha$, where $\tilde{A_B}$ is an empirical factor (with dimensions of an inverse velocity squared), related to the different constants introduced when modeling each element of the gas flux model. By adding this contribution to the nonbreaking parameterization, and considering the transfer velocity normalized to a Schmidt number of 660, k_{w660}, and introducing $A_B = \tilde{A_B}(Sc/660)^{1/2}$ (with $\tilde{A}_B = 1 \pm 0.2 \times 10^{-5}\mathrm{m}^{-2}s^2$ fitted to the data), we obtain the total gas transfer velocity, as a function of the gas diffusivity, solubility, the wind stress, and wave height,

$$k_{w660} = \left(\frac{Sc}{660}\right)^{1/2} k_w = \left(A_{NB}u_* + \frac{A_B}{\alpha}\left[u_*^{5/3}\sqrt{gH_s}^{4/3}\right]\right). \tag{12}$$

Figure 4a and 4b show that this semiempirical relationship collapses all data quite well, with a correlation coefficient squared (R^2) of 0.84 and 0.95 between equation (12) and the 20-min gas transfer measurements from HiWings and Knorr 2011, respectively, and 0.97 and 0.98 for the modeled data for the HiWings and Knorr

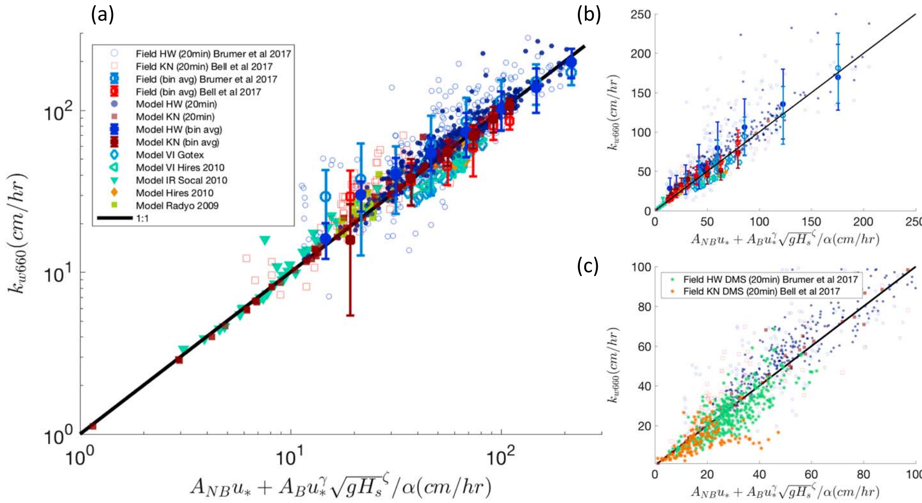

Figure 4. Semiempirical formulation for the gas transfer velocity for CO_2, derived from our complete model, equation (12), $k_{w660} = k_w(Sc/660)^{1/2} = \left(A_{NB}u_* + A_B(u_*^\gamma \sqrt{gH_s}^\zeta)/\alpha\right)$, and $A_B = \tilde{A_B}(Sc/660)^{1/2}$, where $\tilde{A_B} = 1 \pm 0.2 \times 10^{-5}$ $m^{-2} \cdot s^2$ is the only fitted parameter. Exponents $\gamma = 5/3$ and $\zeta = 4/3$ are related to the scaling model for the breaking distribution $\Lambda(c) = Kg^{-1}u_*^\gamma \sqrt{gH_s}^\zeta$, where K is a nondimensional constant. If fitted empirically, the range of exponents $1.5 \leq \gamma \leq 2$, $1 \leq \zeta \leq 1.5$ are acceptable, with $\zeta + \gamma = 3$ constrained by the dimensional scaling of $\Lambda(c)$. The nonbreaking constant is taken as $A_{NB} = 1.55 \times 10^{-4}$ (Fairall et al., 2011); (a) is log scaled, while (b) is linearly scaled. The correlation coefficients squared (R^2) between the semiempirical relationship and the field data are 0.88 and 0.96 for the KN and HW data sets, respectively; 0.9 (KN) and 0.97 (HW) with the modeled data; and 0.85 for the data modeled from measurements of $\Lambda(c)$ and $\phi(k)$. (c) Same plot showing the DMS data from field measurement taken at the same time as the CO_2 data (Bell et al., 2017; Brumer et al., 2017). The DMS data are relatively well described by our semiempirical model, with the bubble term being negligible due to the high solubility of DMS. DMS = dimethyl sulfide; HW = HiWings; IR = infrared measurement of $\Lambda(c)$; KN = Knorr 2011; VI = visible camera measurement of $\Lambda(c)$.

2011 conditions, respectively. For the bin-averaged data, R^2 is above 0.96 for both the measured and modeled data. While these types of relationships are useful, we should emphasize that some scatter is still present, in part because the simple formula does not capture the full complexity of the processes at play, while the spectral formula achieves that to a better extent. Finally, Figure 4c shows that equation (12) holds for DMS, with good comparison with the DMS data from the same field campaigns HiWings and Knorr 2011 (Bell et al., 2013, 2017; Brumer et al., 2017). In the case of DMS, the bubble-mediated term is ~20 times smaller than for CO_2 due to the high solubility, so that the gas transfer is mainly described by the nonbreaking term.

5. Discussion and Conclusion

We have presented a general spectral model for gas transfer that considers the complex dynamics of waves and wave breaking together with a realistic formulation at the bubble scale. We also present a rationale for a simple gas transfer parameterization as a function of wind, friction velocity, and wave height, which collapses all available data. We worked with CO_2, but extension to other gases key to the climate system is straightforward. Indeed, the formula we derived, both the spectral (equation (8)) and semiempirical formulation (equation (12)) include the effects of the gas physicochemical variables, the solubility and diffusivity, which makes it directly applicable to other gas species without changing empirical constants. In the case of highly soluble gases, such as DMS (α about 20 times higher than for CO_2), the outgassing bubble flux becomes much smaller than the nonbreaking gas transfer through molecular diffusion enhanced by turbulence. This comprehensive framework for bubble-mediated gas transfer can easily be implemented in the new generation of coupled ocean-wave models, where all the wave-related information necessary for gas transfer calculations will be available, and should lead to significant reduction in uncertainties related to gas fluxes. The semiempirical relationships can be used with upcoming satellites (e.g., Surface Water and Ocean Topography, SWOT, satellite) where improved spatial resolution of wave properties will be available. We believe that future field work in gas transfer measurements should include more complete measurements of other environmental variables, especially wave directional spectra and Phillips wave breaking statistics to further refine the proposed approach.

Acknowledgments
We thank Ralph Keeling for discussions. L. D. acknowledges support from the Princeton Environmental Institute at Princeton University and the Cooperative Institute for Climate Sciences between NOAA and Princeton University. W. K. M was funded by National Science Foundation grant OCE-1434694 and Office of Naval Research grant N00014-14-1-0710. We thank one anonymous referee for multiple comments that have helped improve the manuscript. Data availability: All field measurements used here have been published previously. All data are available upon request.

References

Aliseda, A., & Lasheras, J. (2011). Preferential concentration and rise velocity reduction of bubbles immersed in a homogeneous and isotropic turbulent flow. *Physics of Fluids*, *23*(9), 093301.

Asher, W., Karle, L., Higgins, B., Farley, P., Monahan, E., & Leifer, I. (1996). The influence of bubble plumes on air-seawater gas transfer velocities. *Journal of Geophysical Research*, *101*(C5), 12,027–12,041.

Banner, M., & Peirson, W. L. (2007). Wave breaking onset and strength for two-dimensional deep-water wave groups. *Journal of Fluid Mechanics*, *585*(1), 93–115.

Banner, M., Zappa, C., & Gemmrich, J. (2014). A note on the Phillips spectral framework for ocean whitecaps. *Journal of Physical Oceanography*, *44*(7), 1727–1734.

Bell, T., De Bruyn, W., Miller, S., Ward, B., Christensen, K., & Saltzman, E. (2013). Air–sea dimethylsulfide (DMS) gas transfer in the North Atlantic: Evidence for limited interfacial gas exchange at high wind speed. *Atmospheric Chemistry and Physics*, *13*(21), 11,073–11,087.

Bell, T. G., Landwehr, S., Miller, S. D., Bruyn, W. J., Callaghan, A. H., Scanlon, B., et al. (2017). Estimation of bubble-mediated air–sea gas exchange from concurrent DMS and CO_2 transfer velocities at intermediate–high wind speeds. *Atmospheric Chemistry and Physics*, *17*(14), 9019–9033.

Brumer, S., Zappa, C., Blomquist, B., Fairall, C., Cifuentes-Lorenzen, A., Edson, J., et al. (2017). Wave-related reynolds number parameterizations of CO_2 and DMS transfer velocities. *Geophysical Research Letters*, *44*, 9865–9875. https://doi.org/10.1002/2017GL074979

Deane, G., & Stokes, M. (2002). Scale dependance of bubble creation mechanisms in breaking waves. *Nature*, *418*, 839–844.

Deike, L., Lenain, L., & Melville, W. K. (2017). Air entrainment by breaking waves. *Geophysical Research Letters*, *44*, 3779–3787. https://doi.org/10.1002/2017GL072883

Deike, L., Melville, W., & Popinet, S. (2016). Air entrainment and bubble statistics in breaking waves. *Journal of Fluid Mechanics*, *801*, 91–129.

Drazen, D. A., Melville, W. K., & Lenain, L. (2008). Inertial scaling of dissipation in unsteady breaking waves. *Journal of Fluid Mechanics*, *611*(1), 307–332.

Edson, J., Fairall, C., Bariteau, L., Zappa, C. J., Cifuentes-Lorenzen, A., McGillis, W. R., et al. (2011). Direct covariance measurement of CO_2 gas transfer velocity during the 2008 Southern Ocean Gas Exchange Experiment: Wind speed dependency. *Journal of Geophysical Research*, *116*, C00F10. https://doi.org/10.1029/2011JC007022

Fairall, C., Bradley, E. F., Hare, J., Grachev, A., & Edson, J. (2003). Bulk parameterization of air–sea fluxes: Updates and verification for the COARE algorithm. *Journal of Climate*, *16*(4), 571–591.

Fairall, C., Yang, M., Bariteau, L., Edson, J., Helmig, D., McGillis, W., et al. (2011). Implementation of the Coupled Ocean-Atmosphere Response Experiment flux algorithm with CO_2, dimethyl sulfide, and O_3. *Journal of Geophysical Research*, *116*, C00F09. https://doi.org/10.1029/2010JC006884

Garbe, C. S., Rutgersson, A., Boutin, J., de Leeuw, G., Delille, B., Fairall, C. W., et al. (2014). *Transfer across the air-sea interface*. (pp. 55–112). Berlin, Heidelberg: Springer Berlin Heidelberg.

Garrett, C., Li, M., & Farmer, D. (2000). The connection between bubble size spectra and energy dissipation rates in the upper ocean. *Journal of Physical Oceanography*, *30*(9), 2163–2171.

Ho, D. T., Law, C. S., Smith, M. J., Schlosser, P., Harvey, M., & Hill, P. (2006). Measurements of air-sea gas exchange at high wind speeds in the Southern Ocean: Implications for global parameterizations. *Geophysical Research Letters*, *33*, L16611. https://doi.org/10.1029/2006GL026817

Ho, D. T., Wanninkhof, R., Schlosser, P., Ullman, D. S., Hebert, D., & Sullivan, K. F. (2011). Toward a universal relationship between wind speed and gas exchange: Gas transfer velocities measured with $^3He/SF_6$ during the southern ocean gas exchange experiment. *Journal of Geophysical Research*, *116*, C00F04. https://doi.org/10.1029/2010JC006854

Jähne, B., Münnich, K., Bösinger, R., Dutzi, A., Huber, W., & Libner, P. (1987). On the parameters influencing air-water gas exchange. *Journal of Geophysical Research*, *92*(C2), 1937–1949.

Katul, G., & Liu, H. (2017). Multiple mechanisms generate a universal scaling with dissipation for the air-water gas transfer velocity. *Geophysical Research Letters*, *44*, 1892–1898. https://doi.org/10.1002/2016GL072256

Keeling, R. F. (1993). On the role of large bubbles in air-sea gas exchange and supersaturation in the ocean. *Journal of Marine Research*, *51*(2), 237–271.

Kleiss, J. M., & Melville, W. K. (2010). Observations of wave breaking kinematics in fetch-limited seas. *Journal of Physical Oceanography*, *40*(12), 2575–2604.

Lamarre, E., & Melville, W. (1991). Air entrainment and dissipation in breaking waves. *Nature*, *351*, 469–472.

Lenain, L., & Melville, W. K. (2017a). Evidence of sea-state dependence of aerosol concentration in the marine atmospheric boundary layer. *Journal of Physical Oceanography*, *47*(1), 69–84. https://doi.org/10.1175/JPO-D-16-0058.1

Lenain, L., & Melville, W. K. (2017b). Measurements of the directional spectrum across the equilibrium saturation ranges of wind-generated surface waves. *Journal of Physical Oceanography*, *47*(8), 2123–2138.

Liang, J.-H., Deutsch, C., McWilliams, J. C., Baschek, B., Sullivan, P. P., & Chiba, D. (2013). Parameterizing bubble-mediated air-sea gas exchange and its effect on ocean ventilation. *Global Biogeochemical Cycles*, *27*(3), 894–905.

Liang, J., McWilliams, J. C., Sullivan, P. P., & Baschek, B. (2011). Modeling bubbles and dissolved gases in the ocean. *Journal of Geophysical Research*, *116*, C03015. https://doi.org/10.1029/2010JC006579

Liang, J.-H., McWilliams, J., Sullivan, P., & Baschek, B. (2012). Large eddy simulation of the bubbly ocean: New insights on subsurface bubble distribution and bubble-mediated gas transfer. *Journal of Geophysical Research*, *117*, C04002. https://doi.org/10.1029/2011JC007766

Liss, P. S., & Merlivat, L. (1986). Air-sea gas exchange rates: Introduction and synthesis. In *The role of air-sea exchange in geochemical cycling* (pp. 113–127). Dordrecht: Springer.

Loisy, A., & Naso, A. (2017). Interaction between a large buoyant bubble and turbulence. *Physical Review Fluids*, *2*(1), 014606.

Miller, S., Marandino, C., De Bruyn, W., & Saltzman, E. (2009). Air-sea gas exchange of CO_2 and DMS in the North Atlantic by eddy covariance. *Geophysical Research Letters*, *36*, L15816. https://doi.org/10.1029/2009GL038907

Nightingale, P. D., Malin, G., Law, C. S., Watson, A. J., Liss, P. S., et al. (2001). In situ evaluation of air-sea gas exchange parameterizations using novel conservative and volatile tracers. *Global Biogeochemical Cycles*, *14*(1), 373–387. https://doi.org/10.1029/1999GB900091

Phillips, O. (1985). Spectral and statistical properties of the equilibrium range in wind-generated gravity waves. *Journal of Fluid Mechanics*, *156*(1), 505–31.

Rapp, R., & Melville, W. (1990). Laboratory measurements of deep-water breaking waves. *Philosophical Transactions of the Royal Society of London. Series A, Mathematical and Physical Sciences*, *331*, 735–800.

Rhein, M., Rintoul, S., Aoki, S., Campos, E., Chambers, D., Feely, R., et al. (2013). Observations: Ocean. In T. F. Stocker, et al. (Eds.), *Climate change 2013: The physical science basis. Contribution of Working Group I to the Fifth Assessment Report of the Intergovernmental Panel on Climate Change* (Tech. rep.). Cambridge, United Kingdom, and New York, NY, USA: Cambridge University Press.

Romero, L., & Melville, W. K. (2010). Airborne observations of fetch-limited waves in the Gulf of Tehuantepec. *Journal of Physical Oceanography*, *40*(3), 441–465.

Romero, L., Melville, W. K., & Kleiss, J. M. (2012). Spectral energy dissipation due to surface wave breaking. *Journal of Physical Oceanography*, *42*, 1421–1441.

Schwendeman, M., Thomson, J., & Gemmrich, J. R. (2014). Wave breaking dissipation in a young wind sea. *Journal of Physical Oceanography*, *44*(1), 104–127.

Sutherland, P., & Melville, W. K. (2013). Field measurements and scaling of ocean surface wave-breaking statistics. *Geophysical Research Letters*, *40*, 3074–3079. https://doi.org/10.1002/grl.50584

Sutherland, P., & Melville, W. K. (2015). Field measurements of surface and near-surface turbulence in the presence of breaking waves. *Journal of Physical Oceanography*, *45*, 943–966.

Thorpe, S. (1982). On the clouds of bubbles formed by breaking wind-waves in deep water, and their role in air–sea gas transfer. *Philosophical Transactions of the Royal Society of London A: Mathematical, Physical and Engineering Sciences*, *304*(1483), 155–210.

Toba, Y. (1972). Local balance in the air-sea boundary processes. *Journal of Oceanography*, *28*(3), 109–120.

Toba, Y. (1978). Stochastic form of the growth of wind waves in a single-parameter representation with physical implications. *Journal of Physical Oceanography*, *8*(3), 494–507.

Toba, Y., Komori, S., Suzuki, Y., & Zhao, D. (2006). Similarity and dissimilarity in air-sea momentum and CO_2 transfers: The nondimensional transfer coefficients in light of windsea Reynolds number. *Atmosphere-Ocean Interactions*, *2*, 53–82.

Wanninkhof, R. (1992). Relationship between wind speed and gas exchange over the ocean. *Journal of Geophysical Research*, *97*(C5), 7373–7382.

Wanninkhof, R., Asher, W., Ho, D., & Sweeney, C. (2009). McGillis, W.Advances in quantifying air-sea gas exchange and environmental forcing.

Wanninkhof, R., & McGillis, W. R. (1999). A cubic relationship between air-sea CO_2 exchange and wind speed. *Geophysical Research Letters*, *26*(13), 1889–1892.

Woolf, D. K. (1997). Bubbles and their role in gas exchange. In *The Sea Surface and Global Change*. Cambridge, UK: Cambridge University Press.

Woolf, D. K. (2005). Parametrization of gas transfer velocities and sea-state-dependent wave breaking. *Tellus B*, *57*(2), 87–94.

Woolf, D., & Thorpe, S. (1991). Bubbles and the air-sea exchange of gases in near-saturation conditions. *Journal of Marine Research*, *49*(3), 435–466.

Zakharov, V. E., Badulin, S. I., Hwang, P. A., & Caulliez, G. (2015). Universality of sea wave growth and its physical roots. *Journal of Fluid Mechanics*, *780*, 503–535.